Supporting Information

Probing the mechanism for bipolar resistive switching in annealed graphene oxide thin films

Pooja Saini,[1†] *Manjri Singh,*[2†] *Jyoti Thakur,*[1] *Ranjit Patil,*[3] *Yuan Ron Ma,*[3] *Ram P. Tandon,*[1] *Surinder P. Singh* [2]* *and Ajit K. Mahapatro*[1]*

[1]Department of Physics and Astrophysics, University of Delhi, Delhi 110007, India.

[2]CSIR-National Physical Laboratory, Dr. K. S. Krishnan Marg, New Delhi 110012, India.

[3]Department of Physics, National Dong-Hwa University, Hualien 97401, Taiwan.

[†] Equal Contributions

*E-mail: amahapatro@physics.du.ac.in, and singh.uprm@gmail.com

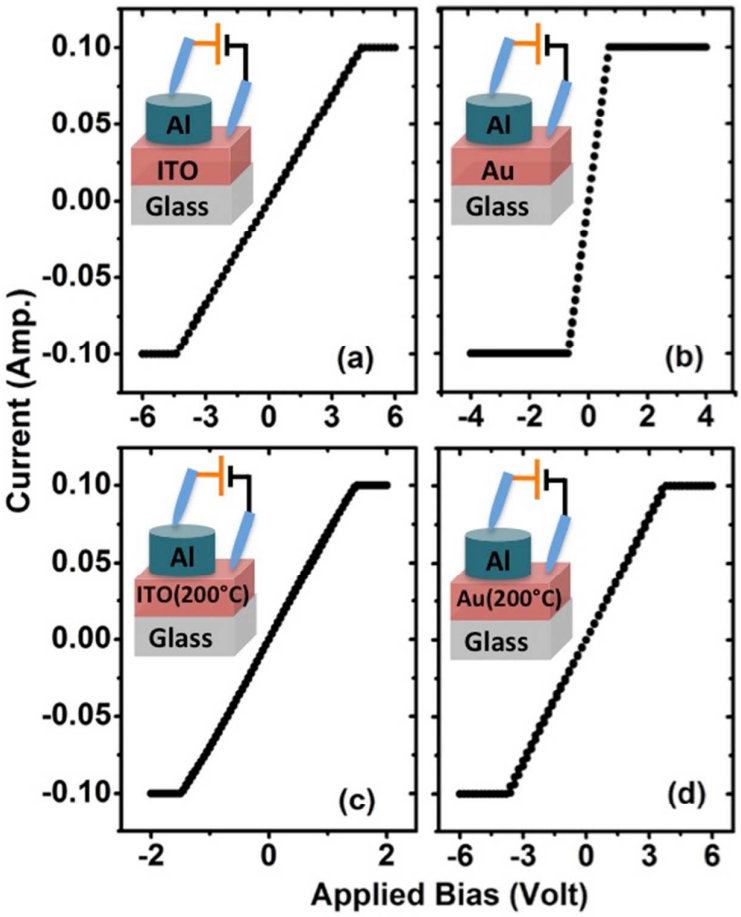

Figure S1. Contact properties of top(M_2)/substrate(M_1)-electrodes: The current-voltage (I-V) characteristics recorded by ramping the voltage in a continuous sweep cycle of $0 \rightarrow +V_{max} \rightarrow 0 \rightarrow -V_{max} \rightarrow 0$ through the structures with M_2(Al)/M_1(ITO,Au) electrode pairs, **(a)** Al/ITO and **(b)** Al/Au, and with substrates (ITO and Au) heated to 200 ^{o}C followed by deposition of top Al contact as **(c)** Al/ITO(200^{o}C) and **(d)** Al/Au(200^{o}C) electrode pairs. All the structures show Ohmic behavior with no sign of hysteresis or switching. The insets show the schematic diagrams of the respective structures with M_1/M_2 electrode pairs. The resistance values of 43, 35, 7, and 15 Ω for the Al/ITO, Al/Au, Al/ITO(200^{o}C) and Al/Au(200^{o}C) structures, respectively.

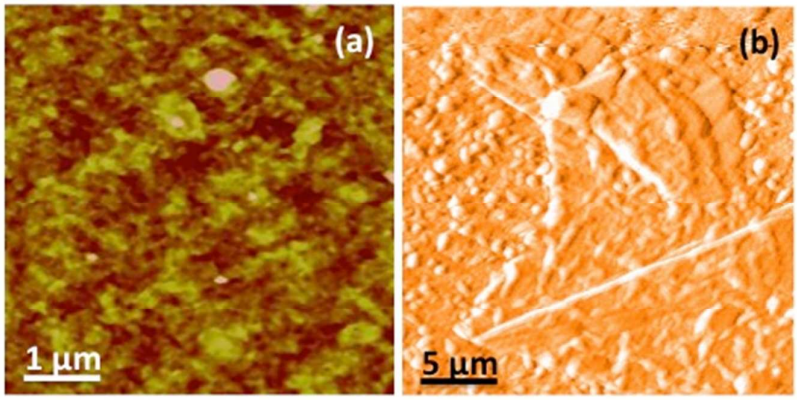

Figure S2. AFM Surface topography of the GO thin films grown on ITO coated glass substrate (GO/ITO) imaged over (a) *5 µm × 5 µm* (b) 2*5 µm × 25 µm* areas.

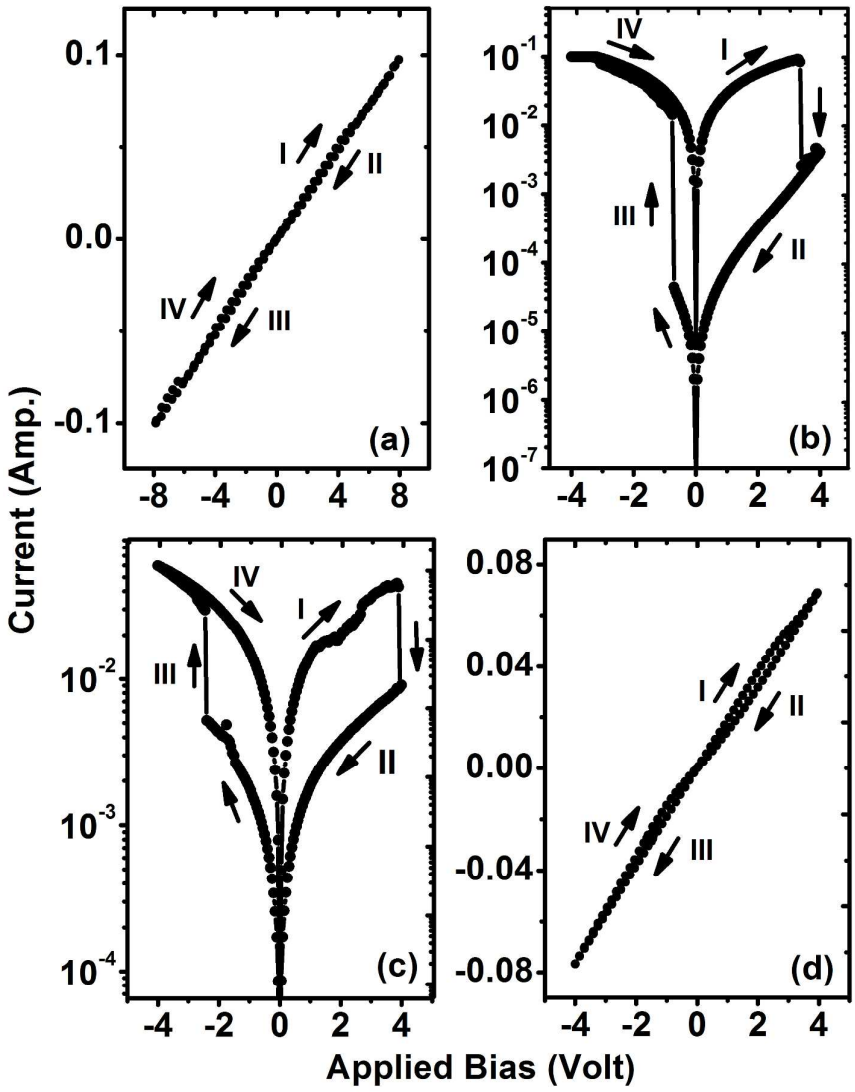

Figure S3. Optimization of the bipolar resistive switching in Al/GO/ITO structures: The current-voltage (I-V) characteristics recorded by ramping the voltage in a continuous sweep cycle of $0 \rightarrow +V_{max} \rightarrow 0 \rightarrow -V_{max} \rightarrow 0$ through **(a)** Al/GO(RT)/ITO, (**b)** Al/GO(100^{o}C)/ITO, **(c)** Al/GO(300^{o}C)/ITO, and **(d)** Al/GO(400^{o}C)/ITO structures. The BRS behavior is prominent in Al/GO(100°C)/ITO and Al/GO(300°C)/ITO structures with switching ratio of (6 ± 4) x 10^{2} and (3.5 ± 0.5) x 10^{1}. The threshold voltages for LRS → HRS and HRS → LRS transitions are observed at V_{+th}= 3.0 ± 0.5 V and V_{-th}= −1 ± 0.5 V for the Al/GO(100°C)/ITO structure, and V_{+th} = 3.8 ± 0.5 V and V_{-th} = −2 ± 0.5 V for the Al/GO(300°C)/ITO structures, respectively. The switching in the Al/GO(RT)/ITO and Al/GO(400°C)/ITO structures are significantly low and unnoticeable.

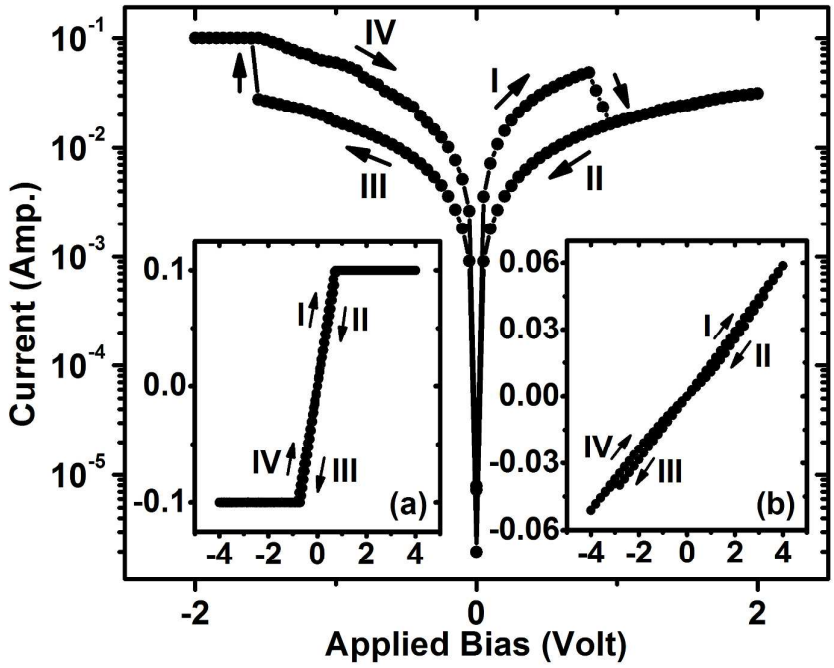

Figure S4. BRS switching only in the device structures with Al as one of the electrodes. Room temperature I-V characteristics recorded through the Al/GO(200°C)/Au, Au/GO(200°C)/Au (**inset 'a'**), and Au/GO(200°C)/ITO (**inset 'b'**) structures, recorded by sweeping the voltage in continuous cycle of $0 \rightarrow +V_{max} \rightarrow 0 \rightarrow -V_{max} \rightarrow 0$, shows BRS is observed only in the Al/GO(200°C)/Au structure and the Au/GO(200°C)/(Au or ITO) structures does not show any sign of switching.

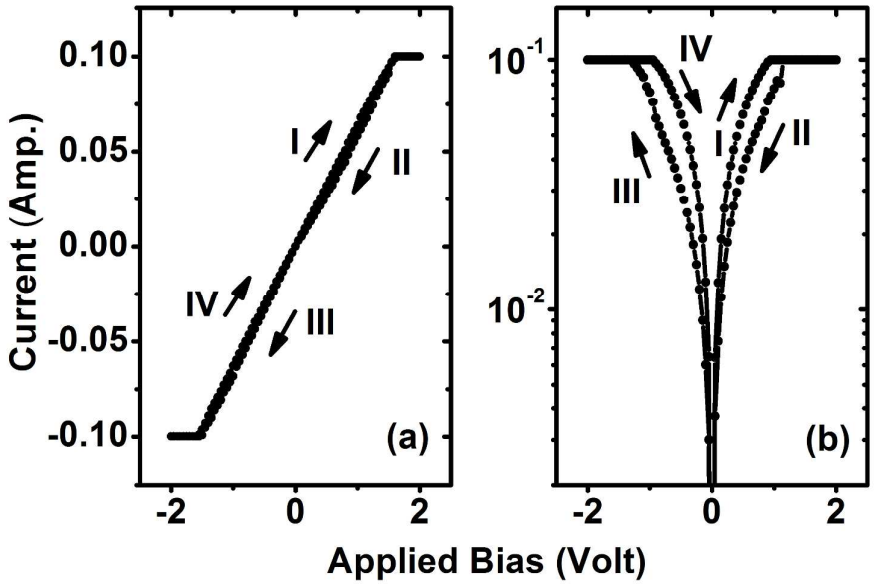

Figure S5. BRS type switching behavior in Al/GO(100°C)/Au device structures: The I-V characteristics recorded by sweeping the voltage in continuous cycle $0 \rightarrow +2V \rightarrow 0 \rightarrow -2V \rightarrow 0$ through the **(a)** Al/GO(RT)/Au (without annealing the GO/Au layer before formation of the Al top electrode) and **(b)** Al/GO(100°C)/Au (by annealing the GO/Au layer at 100°C, before formation of the Al top electrode) structures. No switching in Al/GO(RT)/Au structure and very small BRS behavior in Al/GO(100°C)/Au structure, are observed.

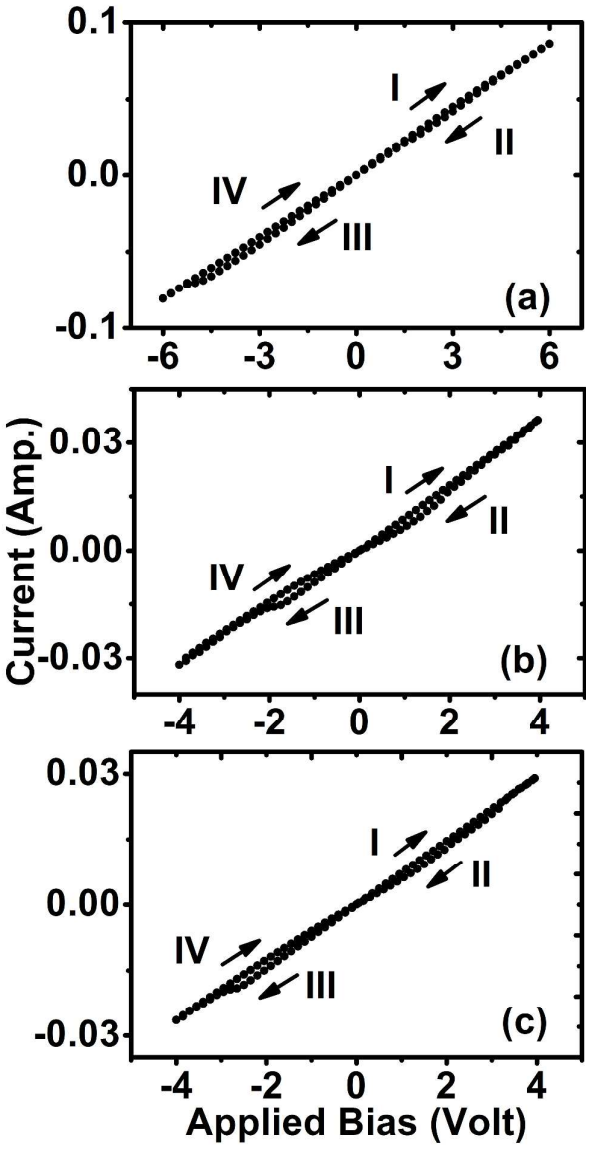

Figure S6. Absence of BRS behavior in Au/GO/ITO device structures: The I-V characteristics recorded by sweeping the voltage in continuous cycle of **(a)** $0 \rightarrow +6V \rightarrow 0 \rightarrow -6V \rightarrow 0$ through Au/GO(RT)/ITO (prepared at room temperature processing) device structure, and $0 \rightarrow +4V \rightarrow 0 \rightarrow -4V \rightarrow 0$for **(b)** Au/GO(300°C)/ITO (fabricated by processing the GO/ITO layers by annealing at 300°C, before the formation of top Au electrode) and **(c)** Au/GO(400°C)/ITO (fabricated by processing the GO/ITO layers by annealing at 400°C, before the formation of top Au electrode) structures. No BRS behavior is observed in all the Au/GO(T)/ITO device structures. The resistance values of 100 ± 10, 170 ± 15, and 200 ± 15 Ω are estimated for the Au/GO(RT)/ITO, Au/GO(300°C)/ITO, and Au/GO(400°C)/ITO device structures, respectively.

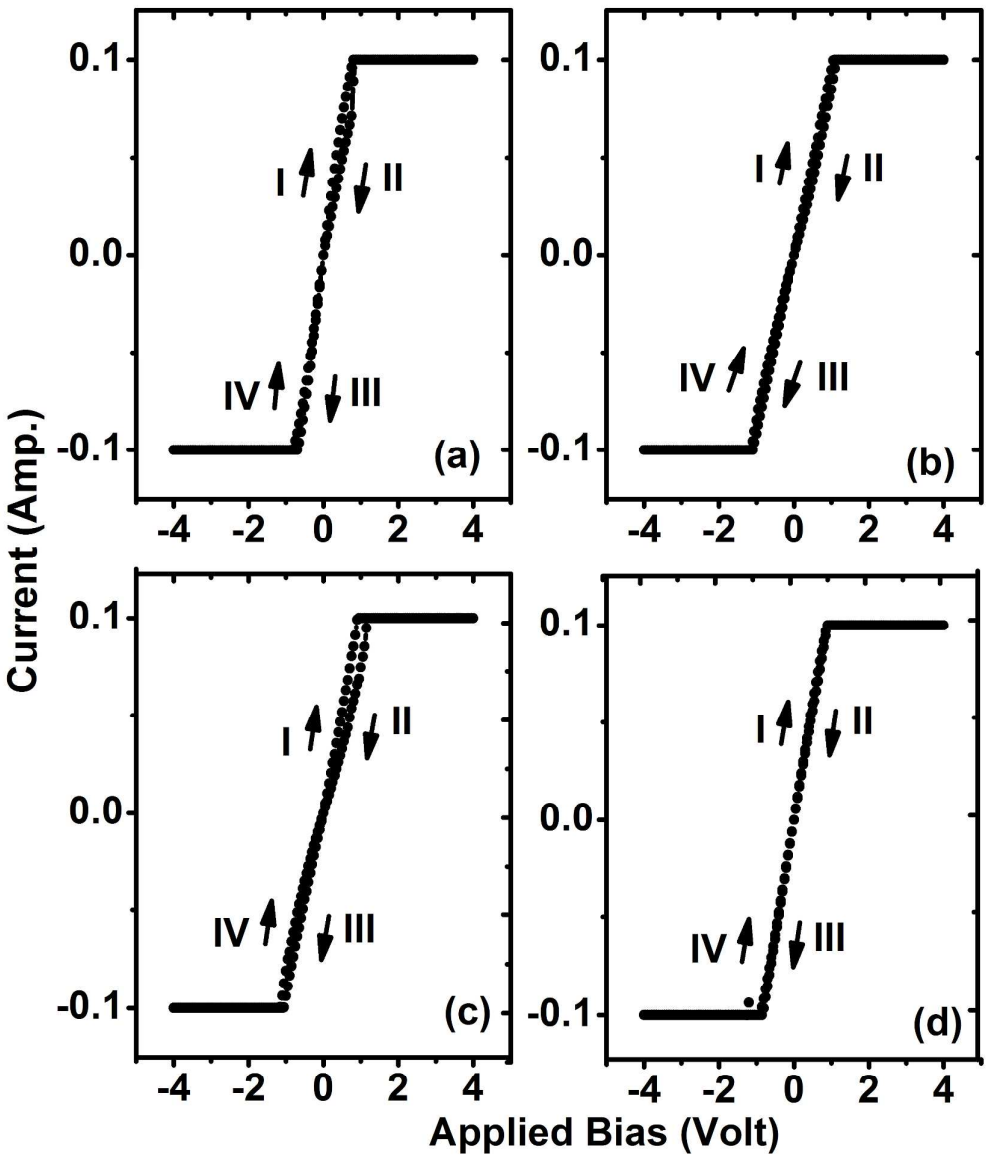

Figure S7. Absence of BRS behavior in Au/GO(T)/Au device structures: The I-V characteristics recorded by sweeping the voltage in continuous cycle in $0 \rightarrow +4V \rightarrow 0 \rightarrow -4V \rightarrow 0$ through Au/GO(T)/Au, device structures prepared at **(a)** room temperature (RT) processing without annealing the GO/Au layers, and by annealing the GO/Au layers at **(b)** 100°C, **(c)** 300°C, and **(d)** 400°C, before the formation of top Au electrode. All the structures show no sign of BRS behavior. The resistance values of 12 ± 1, 7 ± 1, 5 ± 1, and 6 ± 1 Ω are estimated for the Au/GO(RT)/Au, Au/GO(100°C)/Au, Au/GO(300°C)/Au, and Au/GO(400°C)/Au device structures, respectively.

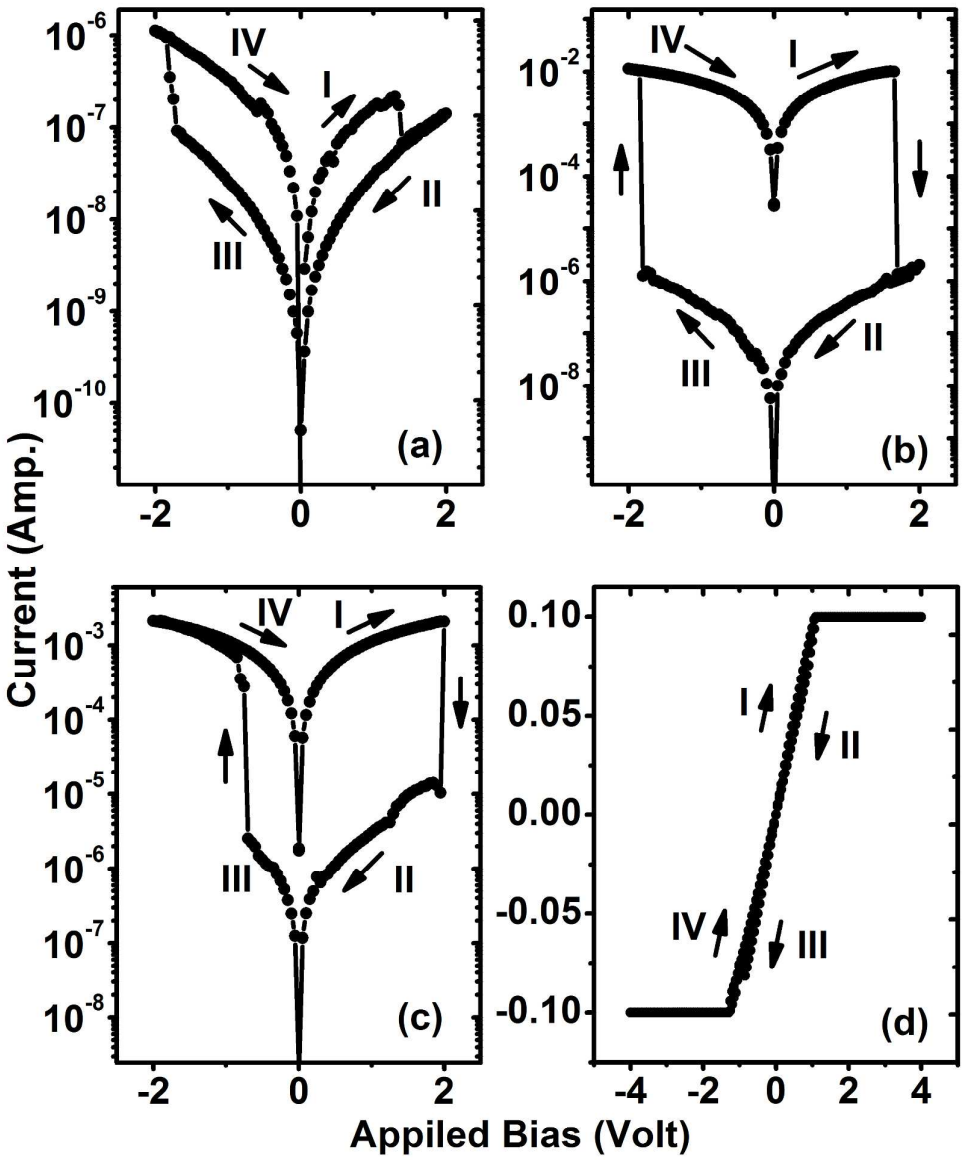

Figure S8. Bipolar resistive switching behavior in Al/GO/Al device structures: I-V characteristics recorded by sweeping the voltage in continuous cycle $0 \rightarrow +V_{max} \rightarrow 0 \rightarrow -V_{max} \rightarrow 0$through the **(a)** Al/GO(RT)/Al, **(b)** Al/GO(100°C)/Al, **(c)** Al/GO(200°C)/Al, and **(d)** Al/GO(300°C)/Al, device structures. Bipolar switching from LRS to HRS during the +ve voltage sweep $0 \rightarrow +V_{max} \rightarrow 0$ and HRS to LRS transition during the –ve voltage sweep $0 \rightarrow -V_{max} \rightarrow 0$ are observed with I_{LRS}/I_{HRS} ratio of ~10^1, ~10^4. ~10^3, and ~10^0 for Al/GO(RT)/Al, Al/GO(100°C)/Al, and Al/GO(200°C)/Al device structures, respectively. The Al/GO(300°C)/Al device structure does not show noticeable BRS behavior.

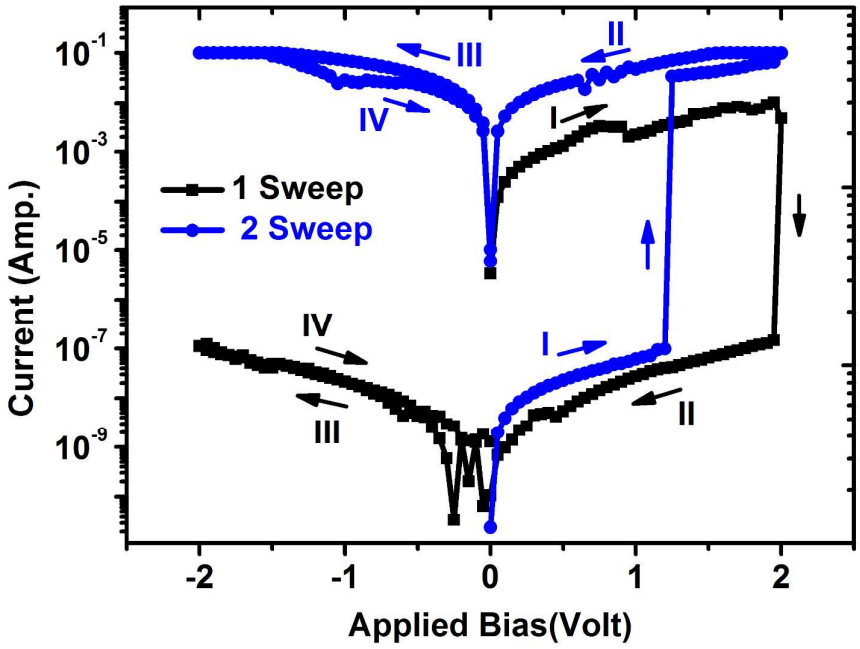

Figure S9. Switching behavior in Al/GO(200°C)/Al device structure: I-V characteristics recorded by sweeping the voltage in continuous cycle $0 \rightarrow +2V \rightarrow 0 \rightarrow -2V \rightarrow 0$through the Al/GO(T200/Al device structures. Ramping the bias from 0V to $+V_{max}$, switching is observed from LRS to HRS at $+V_{th}$, which remains in the same HRS state for rest of the voltage sweep cycle $+V_{+th} \rightarrow +2V \rightarrow 0 \rightarrow -2V \rightarrow 0$. The system regains the original LRS from the HRS during the next sweep cycle $0 \rightarrow +2V \rightarrow 0 \rightarrow -2V \rightarrow 0$and remains in the LRS for rest of the voltage sweep cycle.

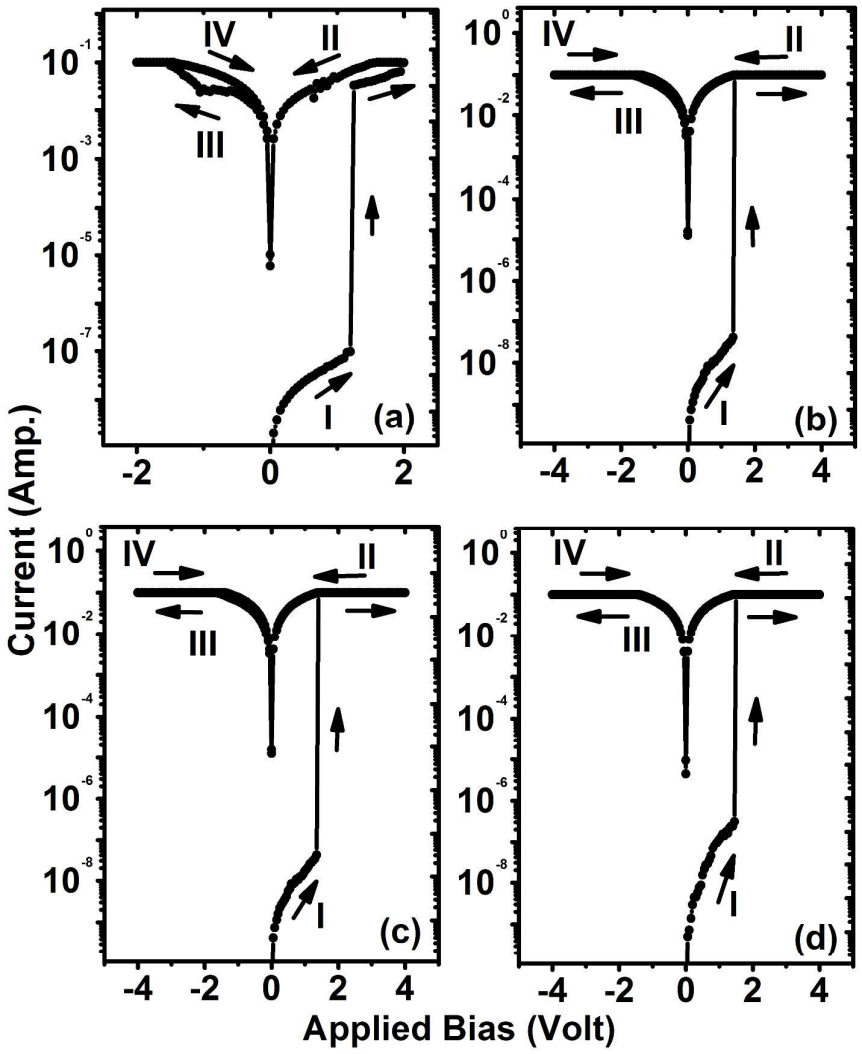

Figure S10. Unipolar switching in Al/GO(T)/Al device structures. I-V characteristics recorded by sweeping the voltage in continuous cycle $0 \rightarrow +V_{max} \rightarrow 0 \rightarrow -V_{max} \rightarrow 0$ through the Al/GO(T)/Al device structures. The **(a)** Al/GO(RT)/Al, **(b)** Al/GO(100°C)/Al, **(c)** Al/GO(200°C)/Al, and **(d)** Al/GO(300°C)/Al devices show unipolar switching from HRS to LRS only in one sweep direction during $0 \rightarrow +V_{max} \rightarrow 0$ (Segment I) and no resistive transition appear in the –ve voltage sweep direction $0 \rightarrow -V_{max} \rightarrow 0$.

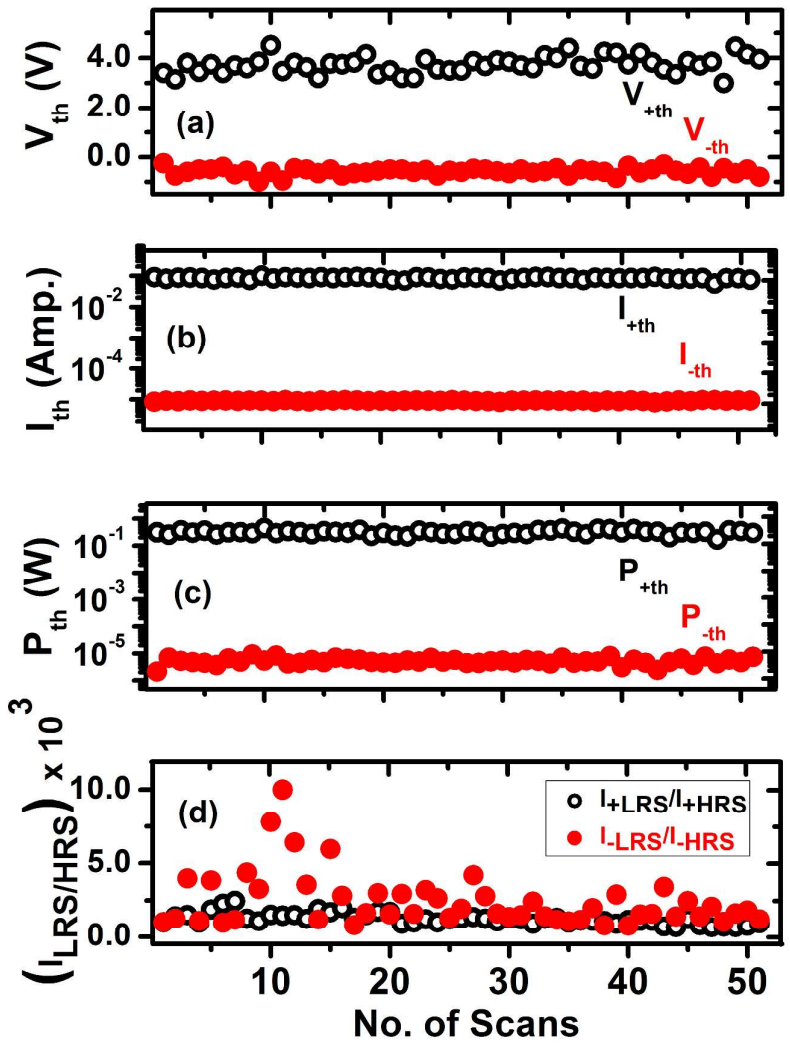

Figure S11. **Variation of $V_{\pm th}$, $I_{\pm th}$, $P_{\pm th}$, and I_{LRS}/I_{HRS} with number of scans for** an individual representative **Al/GO(200°C)/ITO structures.** Variations of **(a)** $V_{\pm th}$, **(b)** $I_{\pm th}$, **(c)** $P_{\pm th}$, and **(d)** I_{LRS}/I_{HRS} observed in consecutive I-V scans through Al/GO(200°C)/ITO structures prepared by following identical recipe. The $I_{\pm th}$ and $P_{\pm th}$ are constant and the $V_{\pm th}$ shows very small variation with number of scans.

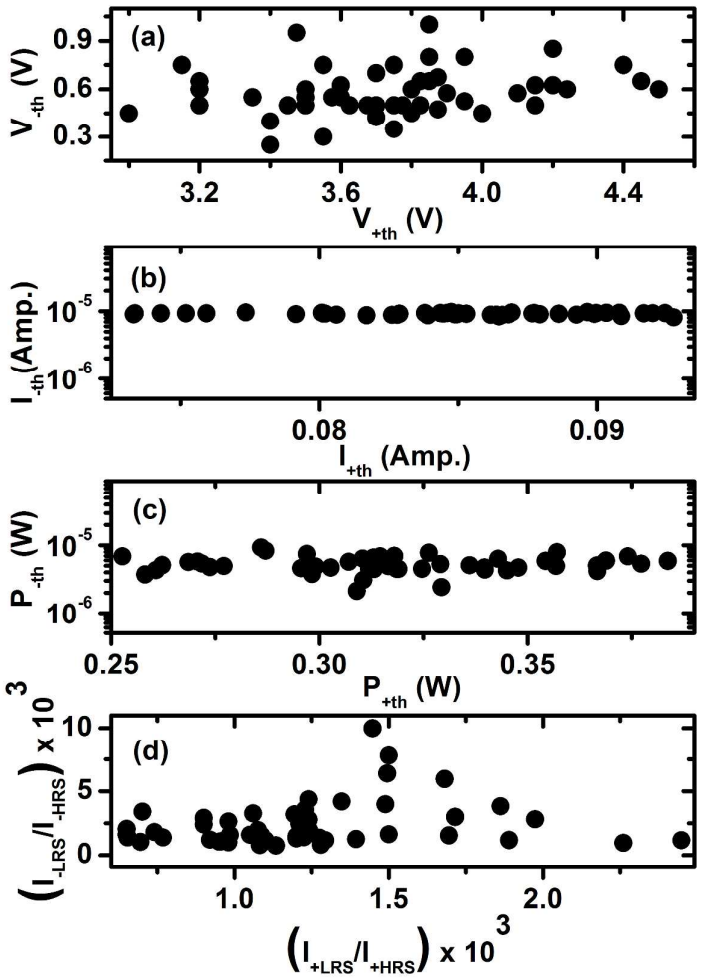

Figure S12. **Dependence of parameters at threshold transition w. r. t. the previous transitions in the other bias scan direction. (a)** Voltage (V_{-th}), **(b)** current (I_{-th}), **(c)** power (P_{-th}), and **(d)** amount of switching (I_{LRS}/I_{HRS}), in reverse bias direction plotted with their corresponding parameters in the forward bias V_{+th}, I_{+th}, P_{+th}, and I_{LRS}/I_{HRS}, respectively. The parameters V_{-th}, P_{-th}, and I_{LRS}/I_{HRS} suggest random values and are in I_{-th}dependently occurring events w. r. t. the previous threshold parameters in the positive bias scan direction. The at the HRS → LRS transition in the –ve bias scan direction $0 \rightarrow -V_{max} \rightarrow 0$, shows occurrence of switching events at the identical current values w. r. t. the corresponding current values at LRS → HRS transitions occurs within a small range of 90 mA.

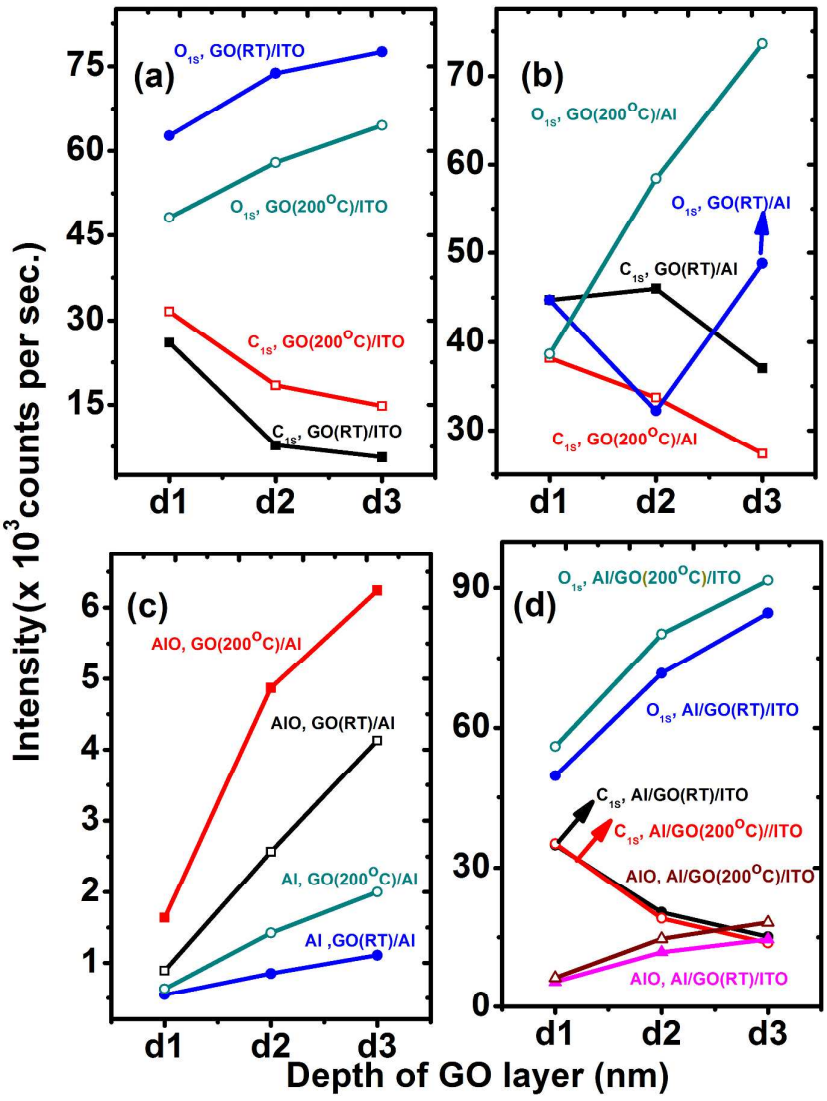

Figure S13. Evolution of the C_{1S}, O_{1S}, AlO in the depth profile XPS spectra. (a) Variation in peak intensities of the C_{1S} and O_{1S} appeared in the depth profile XPS spectra (at d1, d2, and d3 positions) for GO(RT)/ITO and GO(200°C)/ITO layers. The intensity of C_{1S} peak decreases and O_{1S} peak increases with depth, **(b)** The intensities of C_{1S} peak decrease and O_{1S} peak increases with depth in GO(RT)/Al and GO(200°C)/Al layers. **(c)** The intensity of Al and AlO peaks increase with depth in GO(RT)/Al and GO(200°C)/Al layers. **(d)** Variation in the intensities of C_{1S}, O_{1S}, and AlO for Al/GO(RT)/ITO and Al/GO(200ºC)/ITO. The intensity of C_{1S} peak decreases, O_{1S} and AlO(RT) peaks increases, and AlO(200°C) peaks almost constant with depth.

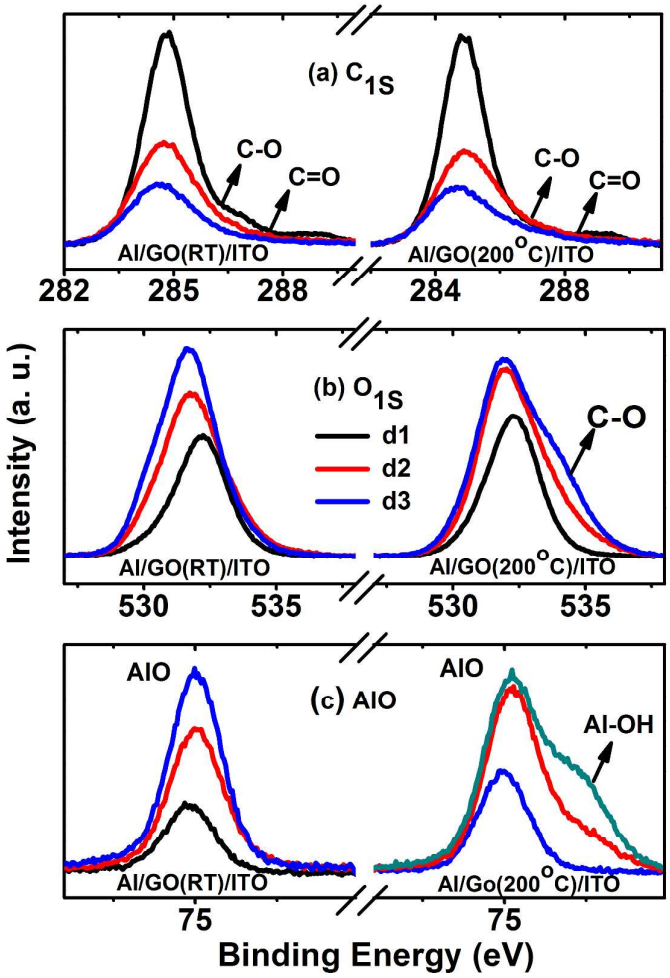

Figure S14. XPS spectra of Al/GO(RT)/ITO and Al/GO(200ºC)/ITO. (a) The depth profile XPS study for Al/GO(RT)/ITO and Al/GO(200ºC)/ITO reveal the C_{1S} signature of reduction of peak intensity at 284.8 eV, and diminishing behavior of C-O and C=O at 286.8 eV and 288.6eV with digging positions of d1, d2, and d3. **(b)** The O_{1S} spectrum indicates peak at 531.7 eV. **(c)** The Al_{2p} spectra shows peak at 74.7 eV due to the presence of AlO that increases with depth (from d1 through d2 to d3) in the Al/GO(RT)/ITO device and remains constant in Al/GO(200°C)/ITO structures. Also, the appearance of a new peak at 76.8 eV for Al-OH increases with depth during digging from d1 through d2 to d3.

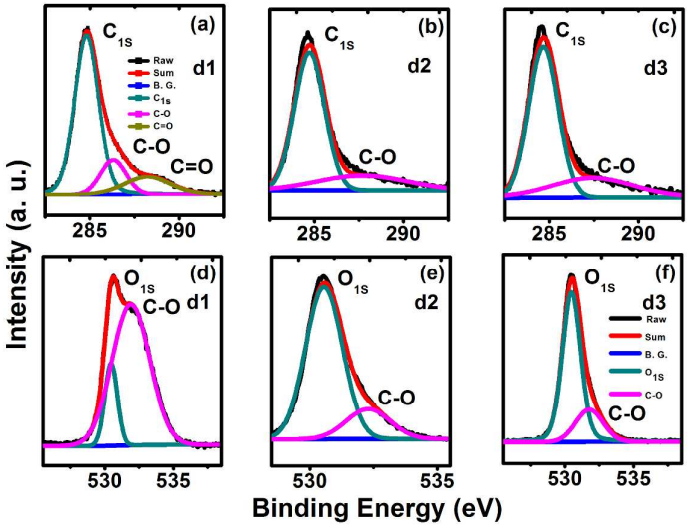

Figure S15. Fitting of XPS spectra for GO(200^{o}C)/ITO. (a) The XPSPEAK v 4.1software provides fitting of C_{1S} spectra with peak position at 284.8 eV, C-O peak at 286.8 eV and C=O at 288.6eV for different depth positions of **(a)** d1, **(b)** d2, and **(c)** d3. The fitting of O_{1S} spectra shows presence of the O_{1S} at 530.1 eV and C-O at 532.3 eV for different depth positions of **(d)** d1, **(e)** d2, and **(f)** d3.

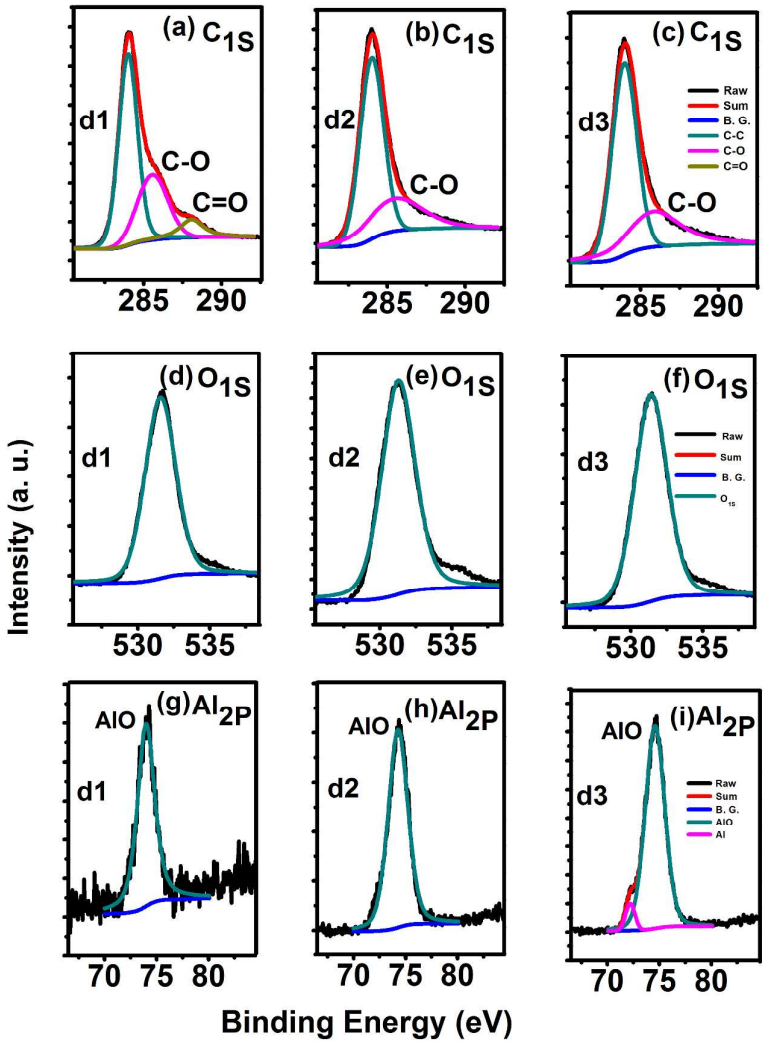

Figure S16. Fitting of XPS for the GO(RT)/Al samples. The XPSPEAK v 4.1 provides C_{1S} spectra with peak position at 284.8 eV, C-O at 286.8 eV and C=O at 288.6eV, for different depth positions of **(a)** d1, **(b)** d2, and **(c)** d3. The C=O peak is diminsihng with digging. The fitting of O_{1S} spectra shows presence of the O_{1S} at 530.1 eV and C-O at 532.3 eV for depth positions of **(d)** d1, **(e)** d2, and **(f)** d3. Fitting of Al2p spectra with peaks of AlO at 74.7 eV and Al at 72.2 eV spectra at **(g)** d1, **(h)** d2, and **(i)** at d3 depth positions.

Characterization of the GO(T)/ITO thin film surfaces using and FTIR spectroscopy [Figure S16]

XRD [Figure S17]

Fourier transform infrared (FTIR) spectroscopy helps identifying the functional groups by locating the vibrational modes in the materials. The structural changes for GO thin films annealed at different temperatures are understood by recording the FTIR spectra and is represented in figure S17. In GO(RT)/ITO, the appearance of vibrational mode at 3323 cm^{-1} corresponds to the O-H stretching vibration from the -OH groups, 1375 cm^{-1} indicates the O-H bending arising due to the presence of water, carboxylic and hydroxyl groups in GO sheets. The peak at 1880 cm^{-1} represents the C=O stretching of carboxylic groups present on the edges of GO sheets and vibrational modes 1065 cm^{-1} is attributed to the stretching vibrations of C-O-C (epoxy, in plane), respectively, and the peak at 1603 cm^{-1} represents the signature of C=C vibrations. The characteristic peaks corresponding to the -OH, C=O, C-O-C, C=C, and C-H vibrational modes suggest the presence of highly pure GO sheets in the GO(RT)/ITO thin films[46, 50]. In annealed GO(T)/RT ($T \geq 200°C$) thin films, the disappearance of vibrational peaks at 3323 cm^{-1}, 1375 cm^{-1}, and 1052 cm^{-1} indicate the removal of oxygen containing -OH, C-O-C epoxy, and C-O-C ether, functional groups in GO sheets of the GO(200°C)/ITO, GO(300°C)/ITO, and GO(400°C)/ITO thin films[49] The increase in the relative intensity of C=C peak 1603 cm^{-1} at higher temperatures of 300^{o}C and 400^{o}C indicates the formation of sp^2 hybridized C-C network, as the higher thermal energies favors clustering of sp^2 carbon. The restoration of sp^2 carbon network is also assisted by formation of Stone-Wales defects by forming 5-8-5 defects (2-pentagon rings and 1-octagon ring) within the hexagon ring structure of GO sheets[50,51].

Figure S18a demonstrates the XRD measurements recorded for GO(T)/ITO surfaces. Here, a prominent diffraction peak at 2θ ~ 10.7° corresponding to the (002) plane of the stacked GO layers[52]is observed in the XRD pattern of GO(RT)/ITO thin films that gradually shifts towards the higher diffraction angles of 10.9 and 12.1 for GO(100°C)/ITO and GO(150°C)/ITO thin films, respectively, and finally disappears with further increasing the annealing temperature above 200 °C, as recorded for the GO(200°C)/ITO, GO(300°C)/ITO and GO(400°C)/ITO thin films. In addition, the appearance of a low intensity broad diffraction peak at 2θ ~ 21.7° in the XRD of GO(RT)/ITO indicates the presence of graphitic domains and poor ordering of the sheets along the stacking direction[53]. The full wave half maxima (FWHM values) for both the peaks are plotted in figure S18b and S18c. The second peak at 2θ ~ 21.7° with very broad FWHM at room temperature gets sharpen with increase in annealing temperatures above 200°C and indicate the restoration of graphitic domains. Here, the initial unchanged FWHM till 150°C is attributed to a mild vaporization of intercalated water molecules and a reduced FWHM above 200°C is due to detachment of other functional groups from the GO flakes, increasing the sp^2 hybridization [54]. This is supported by the reduction of estimated d-spacing values from d_{RT} = 8.1 Å for GO (RT)/ITO to $d_{400°C}$ = 4.2 Å for GO (400°C)/ITO, as calculated by using the Bragg's diffraction formula, $2d \sin\theta = n\lambda$,[55] where, d is the spacing between two planes, ϑ is the diffraction angle, n (= 1) is the constant, and λ (= 1.54 Å) is the wavelength of the incident X-ray beam.

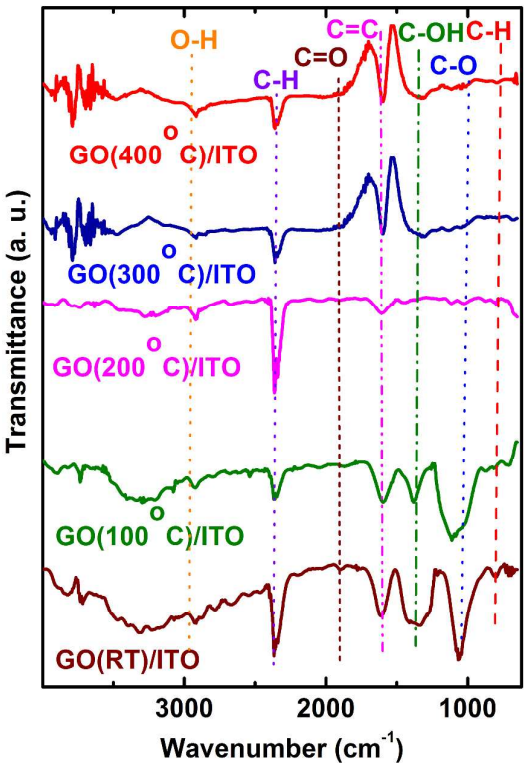

Figure S17. The FTIR spectroscopy at the surfaces of GO(T)/ITO thin films, processed at various annealing temperature, T = RT, 100, 200, 300, and 400 °C. indicates diminishing of peaks assigned for -OH, -CO, C=O groups at higher annealing temperatures above 200 °C.

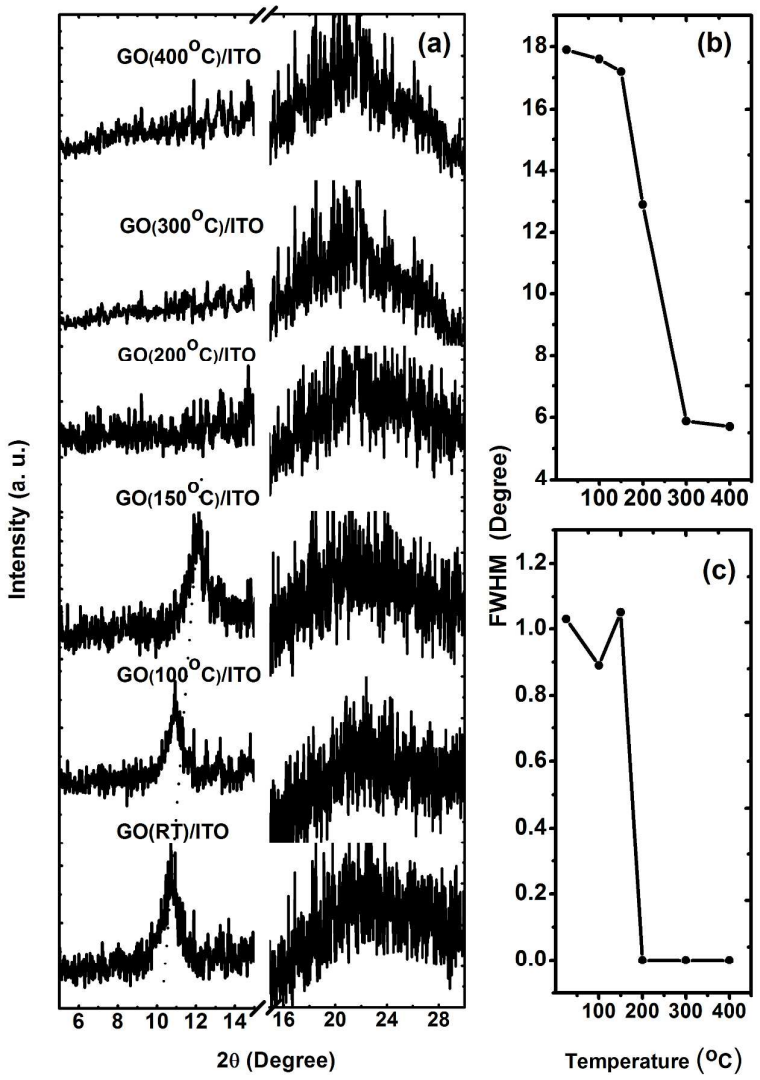

Figure S18. The XRD pattern measured on the surfaces of the GO(T)/ITO thin films, processed at various annealing temperature, T = RT, 100, 150, 200, 300, and 400 °C. (a) Shifting of the characteristic XRD peak for the GO sheets appearing at 2θ = 10.7° towards higher values by increasing the annealing temperature till 200 °C. This peak disappears after annealing the GO layer at and above 200 °C. The Variation in FWHM showing the **(b)** disappearance of the peak at 2θ = 10.7° for GO layers annealed at higher temperatures of 200 °C and above, and **(c)** appearance of broad peak at 2θ = 21.7° that decreases with increasing annealing temperatures indicate sharpened XRD peaks due to formation of GO layers with reduced d-distances of GO-flakes.

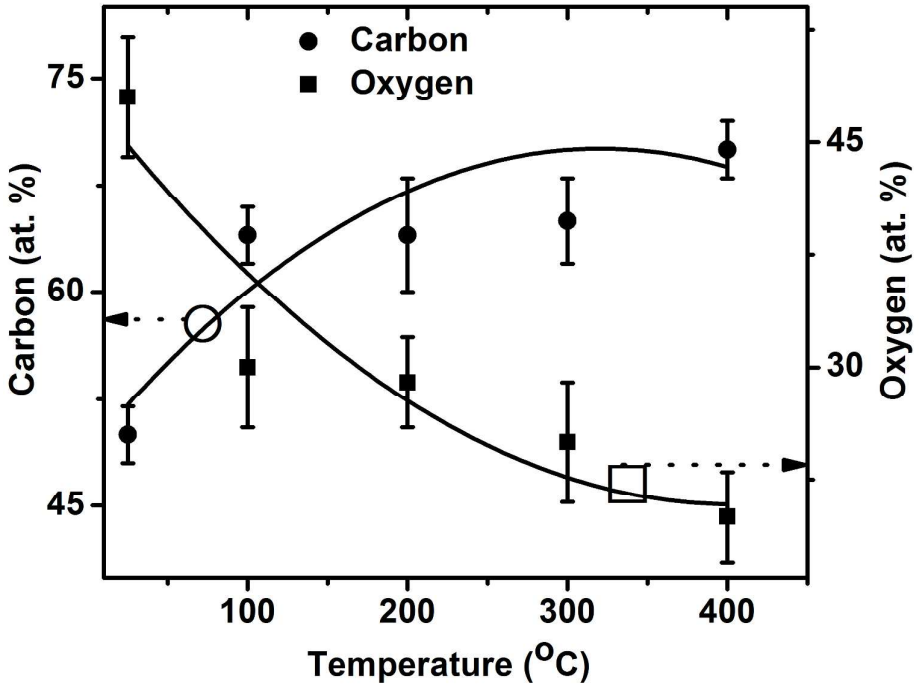

Figure S19. Carbon and oxygen contents in the GO(T)/ITO thin films. The atomic percentages (at. %) for carbon and oxygen contents detected through the EDX attachment to the FESEM for GO(T)/ITO thin films processed at different annealing temperatures of T = RT, 100°C, 200°C, 300°C, and 400°C, indicating increase in the *at.* % of carbon and decrease in the oxygen contents by increasing the annealing temperature.

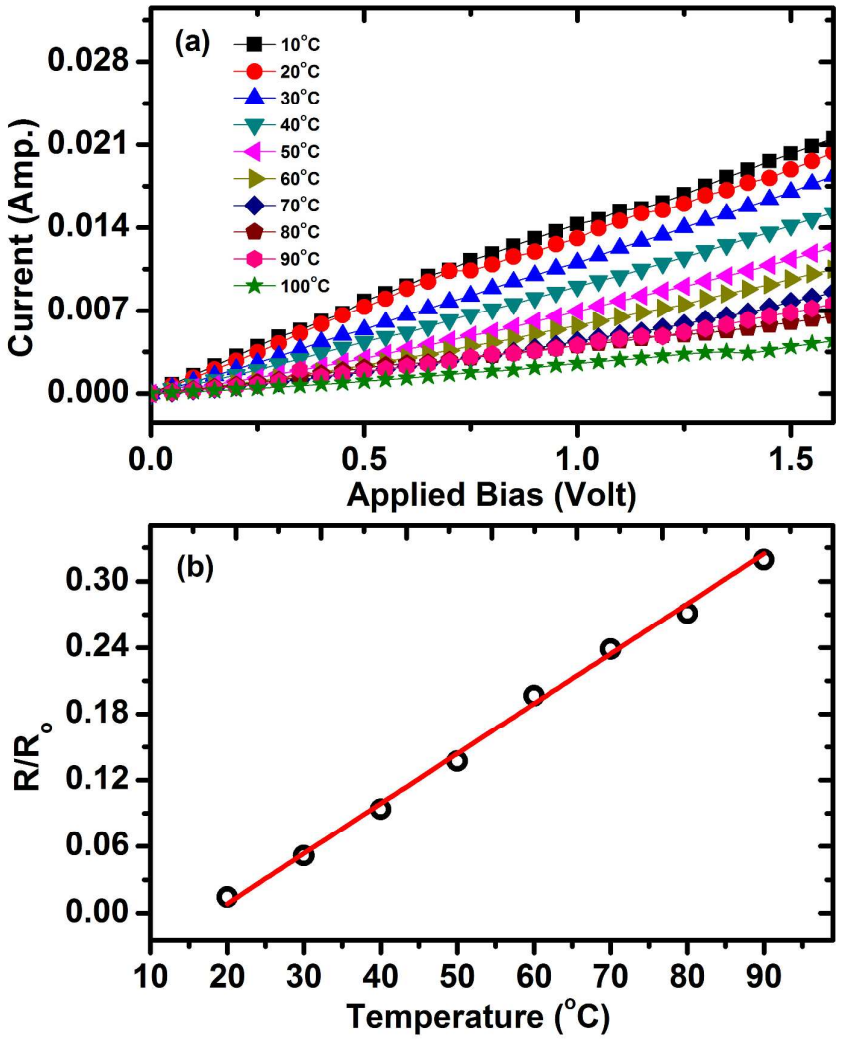

Figure S20. Temperature coefficient of resistance in Al/GO(200ºC)/ITO structure. (a) The I-V characteristics through a representative Al/GO(200ºC)/ITO structure at different temperatures ranging from 10 ºC to 100 ºC, measured with a difference of 10 ºC. **(b)** The R/R_0 values (open circles) estimated for different temperatures indicates a linear fit (continuous line) with the temperature coefficient of resistance, $\alpha = 4.2 \times 10^{-3}$ /ºC.